# The dynamics of a rotor with rubbing

C284/88

# The dynamics of a rotor with rubbing

D de KRAKER, BE, ME, PhD, M T M CROOIJMANS, ME, PhD and D H van CAMPEN, ME, PhD
Department of Mechanical Engineering, Eindhoven University of Technology, Eindhoven, The Netherlands

SYNOPSIS

In real rotor-bearing systems several tight clearances between the rotor and the fixed casing exist. Due to misalignment or excessive unbalances the rotor may rub against the casing. A simple model for this so-called rubbing is introduced. The model consists of a Laval rotor and a non-linear finite boundary stiffness with Coulomb friction.
It is known that rubbing is detected in the vibration spectrum by peaks at integer multiples of the rotorspeed. Therefore, a non-linear calculation technique is used that is based on a periodicity assumption. After discretization with respect to time and using finite differences, the non-linear equations of motion can be transformed into a set of non-linear algebraic equations, which can be solved by standard numerical techniques.
Using an arc continuation method a sensitivity analysis is performed for the system variables. For a particular static deflection of the rotor results are shown of rubbing near the system resonance. Phenomena such as jumping and backward whirl are discussed. Conclusions are drawn for the sensitivity of the phenomena with respect to the boundary stiffness, damping and friction coefficient.

LIST OF SYMBOLS

| | |
|---|---|
| $\sim$ | a tilde denotes a column matrix |
| $\dot{}$ | a dot denotes the first derivative with respect to time |
| $\ddot{}$ | a double dot denotes the second derivative with respect to time |
| ODE | ordinary differential equation |
| $A_0$ | maximum amplitude of rotor response predicted by linear models |
| C | clearance between rotating parts and the fixed housing |
| D | rotor diameter |
| $\vec{e}_x, \vec{e}_y, \vec{e}_z$ | fixed Cartesian triad |
| $F_c^*$ | dimensionless constant force |
| $F_r^*$ | dimensionless coefficient in the expression of the restoring force |
| G | final set of descretized expressions |
| $\tilde{M}$ | rotor mass |
| N | total number of discretization points |
| P | geometrical centre of disc |
| $P^g$ | centre of disc mass |
| $P^m$ | generalized co-ordinates |
| q | |
| $\tilde{R}$ | rotor radius |
| t | time |
| x,y | displacements of the rotor centre |
| $\xi, \eta$ | dimensionless displacements of the rotor centre |
| z | column with unknowns after discretization |
| $\tilde{}$ | |
| $\alpha$ | exponent in expression of the restoring force |
| $\delta$ | parameter that indicates whether the rotor touches the housing |
| $\varepsilon$ | dimensionless mass eccentricity |
| $\varsigma$ | dimensionless damping of the rotor support |
| $\theta$ | angle defined by eq. (3) |
| $\tau$ | dimensionless time |
| $\omega$ | dimensionless rotor speed |
| $\omega_o$ | dimensionless frequency at $A_0$ |
| $\Omega$ | constant rotational rotor speed |

## 1 INTRODUCTION

In real rotors narrow clearances between the rotating parts and the fixed housing exist. In the ideal situation clearances between the fixed and rotating parts are circumferentially equal. Generally, this is not true due to misalignment; furthermore, the rotor is excited by mass unbalance and will vibrate. Due to this combination the rotating parts may rub against the housing and cause very different dynamic

behaviour that is usually difficult to predict. However, it was recognized that due to rubbing the rotor vibrates periodically or quasi-periodically. In the vibration spectrum this can be identified by sharp peaks at a restricted number of frequencies and their multiples (lit. [2, 3, 4, 5]). In this paper we will assume that the rotor vibrates periodically.
We will analyse the dynamic behaviour of a simple model consisting of a Laval rotor and a massless boundary with a non-linear restoring force.
The mathematical model results in two coupled second order ODE's. The number of design variables can be reduced by using a non-dimensional form of the set of ODE's. We will assume that the rotor touches the static parts slightly and the sensitivity of the response with respect to the various design variables will be investigated.

## 2 ROTOR GEOMETRY, CONSTANT LOAD AND ISOTROPIC SUSPENSION

The Laval rotor has been modelled as a massless shaft mounted in two bearings at each end. Symmetrically between the bearings, it has an infinitely thin rigid disc perpendicular to the shaft. The disc has a mass M and radius R, whilst it rotates with a constant angular velocity $\Omega$ around the centre $P_g$ of the disc. The centre of mass $P_m$ of the disc does not necessarily coincide with $P_g$ as indicated in figure 1a.
The bending vibrations of this rotor have been modelled with two generalized co-ordinates. In the reference configuration, $P_g$ coincides with the origin $P_o$ of the Cartesian triad ($\vec{e}_x$, $\vec{e}_y$, $\vec{e}_z$). The disc translates in the $\vec{e}_x$- and $\vec{e}_y$-directions and rotates around the direction of $\vec{e}_z$. The position of $P_g$ with respect to $P_o$ is given by the vector $\vec{r}_g$ and the position of $P_m$ with respect to $P_g$ by $\vec{r}_e$. $\vec{r}_g$ and $\vec{r}_e$ are expressed in terms of $\vec{e}_x$ and $\vec{e}_y$ as follows:

$$\vec{r}_g = x\vec{e}_x + y\vec{e}_y$$
$$\vec{r}_e = e\cos(\Omega t)\vec{e}_x + e\sin(\Omega t)\vec{e}_y \qquad (1)$$

Where x and y are generalized co-ordinates, e is the distance between $P_m$ and $P_g$ while $\Omega t$ is the rotation angle.
The disc is loaded with a constant force $\vec{F}^c$, a load $\vec{F}^l$ that is linearly dependent on the generalized co-ordinates, and a non-linear load $\vec{F}^r$. The constant load $\vec{F}^c$ with amplitude $F_c$ points into the negative y-direction.
The linear force $\vec{F}^l$ results from isotropic stiffness, $k_s$, and isotropic damping, $d_s$, of the shaft and its bearings and it acts at $P_g$.

## 3 RUBBING FORCES

The non-linear load $\vec{F}^r$ is produced by the rubbing of the rotor against the stationary housing. We assume that during the motion of the rotor the housing only adds stiffness to the rotor. In the reference configuration, the clearance between the disc and the housing is constant and is called C. We can formulate a condition in which the disc contacts the housing:

$$\sqrt{(x^2+y^2)} \geq C \text{ or } \delta = \sqrt{(x^2+y^2)}/C - 1 \geq 0 \qquad (2)$$

We assume that the disc and the housing make contact at one point $P_r$ only if the contact criterium (2) is fulfilled. The position of point $P_r$ relative to $P_o$ is given by the vector $\vec{r}_p$:

$$\vec{r}_p = (R+C)(\cos\Theta\,\vec{e}_x + \sin\Theta\,\vec{e}_y) \qquad (3)$$

with: $\tan\Theta = y/x$

The housing acts on the disc with a normal force $\vec{F}^t$ and a tangential or friction force $\vec{F}^w$ (figure 1b). We assume that the normal force depends on $\delta$ exponentially:

$$\vec{F}^t = \vec{F}^t_x + \vec{F}^t_y = \begin{cases} \vec{0} & \text{if } \delta<0 \\ -F_r\delta^\alpha(\cos\Theta\,\vec{e}_x + \sin\Theta\,\vec{e}_y) & \text{if } \delta\geq 0 \end{cases} \qquad (4)$$

In (4), we represent the normal force by means of a positive constant $F_r$ and an exponent $\alpha$. If $\alpha > 1$, the normal force as a function of $\delta$ has a continuous first derivative. Physically, the rotor presses against the housing. Instantaneously, this will cause a local impression of the housing. The normal force needed for this impression increases non-linearly with the magnitude of the impression.
The friction force $\vec{F}^w$ is represented by Coulomb's law with the characteristic Coulomb friction coefficient f:

$$\vec{F}^w = \vec{F}^w_x + \vec{F}^w_y = \begin{cases} \vec{0} & \text{if } \delta<0 \\ f\,F_r\delta^{\alpha}(\sin\Theta\,\vec{e}_x - \cos\Theta\,\vec{e}_y) & \text{if } \delta\geq 0 \end{cases} \quad (5)$$

In this model, we have assumed that the relative velocity of the rotor contact point with respect to the housing contact point is always counterclockwise and unequals 0. This assumption was checked and appeared to be valid for the results that we will show later. With (4) and (5), we can find $\vec{F}^r$ from $\vec{F}^r = \vec{F}^t + \vec{F}^w$.

## 4 EQUATIONS OF MOTION

We are now able to formulate the equations of motion using Newton's law:

$$M\,\ddot{\vec{r}}_m = M\,(\ddot{\vec{r}}_g + \ddot{\vec{r}}_e) = \vec{F}^c + \vec{F}^l + \vec{F}^r \quad (6)$$

This can be transformed in two coupled ODE's.

$$M\,(\ddot{x} - e\Omega^2\cos(\Omega t)) = -d_s\dot{x} - k_s x + \underline{F_r\delta^{\alpha}(-\cos\Theta + f\sin\Theta)} \quad (7a)$$

$$M\,(\ddot{y} - e\Omega^2\sin(\Omega t)) = -F_c - d_s\dot{y} - k_s y + \underline{F_r\delta^{\alpha}(-\sin\Theta - f\cos\Theta)} \quad (7b)$$

The underlined terms in the equation (7) have to be taken into account only when $\delta\geq 0$.

The number of design variables in equation (7) is eleven. We will reduce this number by writing these equations in a non-dimensional form. For this purpose, we must define a characteristic frequency $\omega_k$ as: $\sqrt{k_s/M}$. Furthermore, we will use the clearance C as a characteristic length of the problem. With C and $\omega_k$ we can define a number of non-dimensional variables:

$$\begin{aligned} (\xi,\eta) &= (x/C, y/C) \quad ; \varepsilon = e/C \\ \tau &= \omega_k t \quad ; \omega = \Omega/\omega_k \\ \varsigma &= d_s/(2M\omega_k) \\ F^*_r &= F_r/(MC\omega_k^2) \quad ; F^*_c = F_c/(MC\omega_k^2) \end{aligned} \quad (8)$$

If we use (8) for rewriting equation (7), we obtain:

$$\xi'' + 2\varsigma\,\xi' + \xi + \underline{F^*_r\delta^{\alpha}(\cos\theta - f\sin\theta)} = \varepsilon\omega^2\cos\omega\tau \quad (9a)$$

$$\eta'' + 2\varsigma\,\eta' + \eta + \underline{F^*_r\delta^{\alpha}(\sin\theta + f\cos\theta)} = -F^*_c + \varepsilon\omega^2\sin\omega\tau \quad (9b)$$

with: $(\,)' = d(\,)/d\tau$ , $(\,)'' = d^2(\,)/d\tau^2$

## 5 SOLUTION METHOD

A method is discussed which provides periodic solutions of the non-linear equations of motion (9) as a function of any of the design variables. This method is based on time discretization of the system equations combined with a numerical solution algorithm to solve the resulting non-linear algebraic equations.

Instead of a continuous periodic solution of the equations (9) an approximate solution at a discrete number of times will be determined. In order to discretise the equations (9) let $\tau_j$ (j=1,...,N) be an equidistant partition of one period of time T, yielding:

$$\tau_j = \frac{(j-1)}{N}\,T \quad (10)$$

with T the period of time that results from $\Omega$ ($T = 2\pi/\Omega$). The velocity and acceleration in the direction of $\vec{e}_x$ at $\tau_j$ are expressed with a 4th order central difference scheme. The velocity and the acceleration in the direction of $\vec{e}_y$ at $\tau_j$ can be expressed in a similar way.

Application of these discretization schemes in the equations of motion at the N discretization points yields 2N algebraic equations. The algebraic equations are denoted by:

$$\underset{\sim}{G}\,(\underset{\sim}{z}) = \underset{\sim}{0} \quad (11)$$

with the 2N unknowns:

$$\underset{\sim}{z}^t = [\xi(\tau_1),\ldots,\xi(\tau_N),\eta(\tau_1).,,,.\eta(\tau_N)] \quad (12)$$

This set of algebraic equations can be solved by a standard multi-dimensional Newton-Raphson method. If we add one of the variables as an unknown we can solve the equations with an arc continuation method [1], and obtain solutions as a function of that variable.

The operation of the arc continuation method is based on a prediction step followed by correction steps until the solution at a next value of the design variable is reached.

In order to find an initial solution with which we can start the Newton Raphson procedure, a

first calculation with the linearized set of equations can be made. The resulting solution will resemble the solution of the set of non-linear ODE's as long as the excitational forces in (9) are small.

## 6 DESCRIPTION OF THE BEHAVIOUR AS A FUNCTION OF ROTOR SPEED

If we neglect the stiffness of the housing a simple set of linear ODE's remain from (9). We will refer to this situation as the linear case whereas the non-linear case will mean that we do take into account the non-linear restoring force of the housing. Both the radial frequency, $\omega_o$, and the corresponding vibration amplitude ($A_o$) at resonance can be solved analytically for the linear case.

We will assume that the static equilibrium position $(\xi,\eta)$ of the rotor centre $P_g$ due to $F_c^*$ is at $P_2=(0,-0.9)$. Additional dynamic loads will cause the rotor to rub against its housing.

We have assumed a low damping value of $\varsigma=0.02$. The choice of $\varepsilon=0.008$ was made so that rub will occur. At this value the maximum amplitude of the rotor for the linear case is $A_o=0.2$ The housing characteristics were $F_r^*=10$, $\alpha=1.3$ and $f=0.20$.

Figure 2 shows the amplitude of the rotor vibration as a function of the rotor speed, in both the linear and non-linear cases. The amplitude of the non-linear periodic motion has been calculated as half of the maximum minus the minimum value of both the x- and the y-co-ordinates. The amplitude of the x- and y-co-ordinates of the linear curve are equal. At each of the symbols (Δ, o, etc.) the periodic solution has been determined using the arc continuation method. Some of the points at the amplitude curve of the x-co-ordinate have been numbered.

The differences between linear and non-linear forced response functions are obvious. The peaks of the x- and y-amplitudes are both at higher frequencies than the linear resonance frequency $\omega_0$. The amplitudes are larger as well. An increase of the resonance frequency was to be expected from the increase of the stiffness produced by the housing.

In figure 3, the motion of $P_g$ has been drawn in the x-y plane for the calculated points indicated in figure 2. The arrows indicate the whirl-direction of the rotor.

If we slowly increase the rotor speed, the rotor will hit the housing at (0,-1) for the first time. From that point the orbit in the x-y plane will deviate from the circular form that follows from linear analysis. The increasing y-amplitude is restricted by the housing. At points 8 to 17, the rotor centre $P_g$ whirls in the same direction as the rotor speed.

At points 19 to 33, the rotor whirls backward, which is caused by the frictional force. In its final part, the motion will approache a circular form when the rotor no longer touches the housing.

In practice, the motions at the equilibrium points 23 to 43 will never occur because they appeared to be unstable as confirmed by numerical time integration. If we slowly increase the rotor speed, the motion will jump suddenly from near point 23 to a motion where the rotor does not touch the housing.

## 7 INFLUENCE OF THE DAMPING

The shape of a resonance peak of a linear system depends greatly on the dimensionless damping coefficient $\varsigma$. When the damping increases, $A_0$ decreases, $\omega_0$ increases and the peak becomes less sharp.

Starting from the non-linear results shown in figure 2 we can vary the damping $\varsigma$ at four levels: $\varsigma=0.02$, $\varsigma=0.05$, $\varsigma=0.10$ and $\varsigma=0.20$. The corresponding linear amplitude $A_0=0.2$ was kept constant by adjusting the eccentricity value $\varepsilon$; $\varepsilon$ was 0.008, 0.01998, 0.0398 and 0.0784 respectively. Figure 4 shows the results of these successive cases.

With an increased damping, a larger unbalance $\varepsilon$ was chosen in order to keep the same value of $A_0$. In this case, the magnitude of the unbalance forces increases as compared with the magnitude of the restoring forces of the housing. For large values of $\varsigma$, and thus of $\varepsilon$, the solution resembles the linear solution more and more. Also, after increasing the damping, its stabilizing effect increasingly dominates the destabilizing frictional forces. The unstable series of solutions will disappear entirely for large damping values. Also, the unstable backward whirl motion will not exist any longer for $\varsigma=0.10$.

The jump phenomenon that occurs when the rotor

speed is slowly increase, does not necessarily disappear when we increase the damping. In figure 4, we observe the largest jump at a damping level of $\varsigma$=0.10.

## 8 INFLUENCE OF HOUSING STIFFNESS AND FRICTION COEFFICIENT

The stiffness of the housing can be changed by varying both $\alpha$ and $F_r^*$. Figure 5a shows the effect of an increase of $\alpha$ for both the amplitudes of the x- and y-co-ordinates. A decreased stiffness leads to a reduced resonance frequency. It also diminishes the unstable series of solutions. Due to the increased stiffness, the contact time between the rotor and the housing decreases. Therefore, the friction forces will have less influence and the backward whirl will eventually disappear. The jump in the y-co-ordinate amplitudes decreases too, while varying $F_r^*$ leads to similar results.
The influence of a variation in the Coulomb friction coefficient f on the stationary behaviour is shown in figure 5b. In this example, the frictional forces point mainly in the x-direction. Therefore, the largest influence can be expected in the x-direction too as can be observed in figure 5b. The frictional forces diminish with f and, thus, the amplitude of the x-co-ordinate increases.

## 9 CONCLUSIONS

A rotor model was introduced that took into account rubbing between the rotating part and the stationary part. The reaction of the housing was modelled by a non-linear restoring force and a friction force. In the dimensionless form, the design variables for the model were varied in order to investigate their influence. For all results the resonance frequencies increase compared to those in the corresponding linear case due to the added housing stiffness. In the spectrum of the periodic solutions higher harmonics are found in addition to the first harmonic that can be found from linear analysis. In slightly damped cases, a backward whirl is caused by the friction force. However, it is found that this backward whirl is never stable. With the aid of numerical time integration, we learn that increasing or decreasing the rotor frequency causes the rotor to jump from one rotor orbit to another. A series of unstable periodic solutions are then passed over.
Results obtained for a rotor that rubbed the housing slightly are sensitive to the damping. Therefore, we adjusted the mass unbalance in such a way that the system without the housing had a constant maximum amplitude for all damping levels. From these results, we conclude that when the damping increases, the influence of the housing decreases and the backward whirl finally disappears. However, a greater damping does not necessarily mean that the jump phenomenon is less pronounced.
An increased housing stiffness leads to somewhat higher resonance amplitudes and frequencies. An increased friction coefficient has little influence on the results.

## ACKNOWLEDGEMENT

These investigations were supported (in part) by the Netherlands Foundation of Technical Research (STW). The authors are indebted to Professor W.L. Esmeijer for valuable discussions and contributions to this paper.

## REFERENCES

[1] Fried I., Orthogonal trajectory accession to the nonlinear equilibrium curve, Computer Methods in Applied Mechanics and Engineering, Vol. 47, 1984, pp 283-297.

[2] Crooijmans, M.T.M., On the Computation of Stationary Deterministic Behaviour of Non-Linear Dynamic Systems with Application to Rotor-Bearing structures, Thesis, University of Technology Eindhoven, oktober 1987.

[3] Beatty R.F., Differentiating rotor response due to radial rubbing, Journal of Vibration, Acoustics, Stress and Reliability in Design, April 1985. Vol. 107, pp 151-159.

[4] Muszynska, A., Nonlinear excited and self-excited processional vibrations of symmetrical rotors, Dynamics of rotors (Symposium Denmark), 12-16 augustus 1974, Springer Verlag, Berlin 1975.

[5] Childs, D., Fractional-frequency rotormotion due to nonsymmetric clearance effects, Journal of Engineering for Power, july 1982, Vol. 104, pp 533-541.

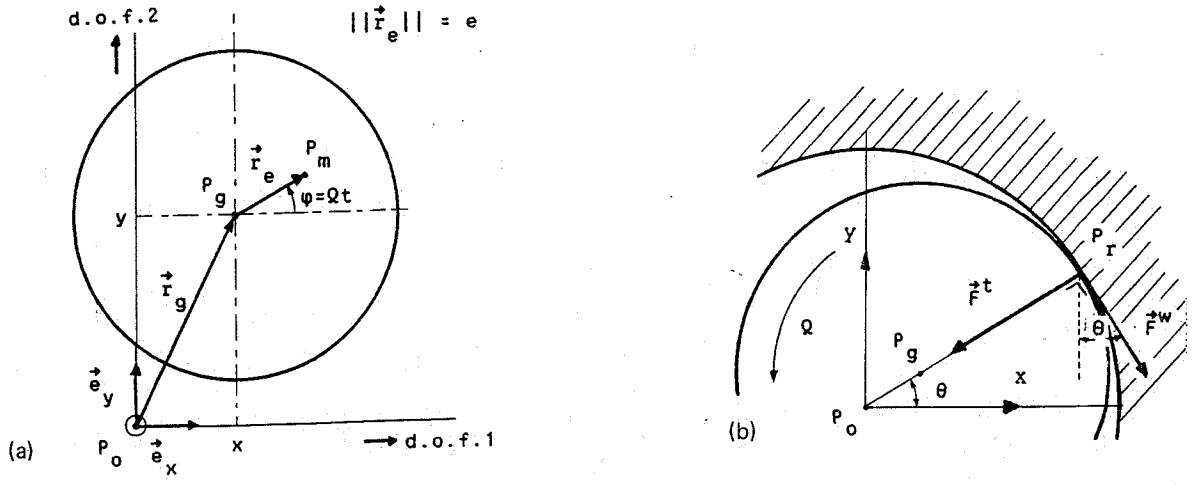


Fig 1 Degrees of freedom of the Laval rotor (a) and rubbing forces (b)

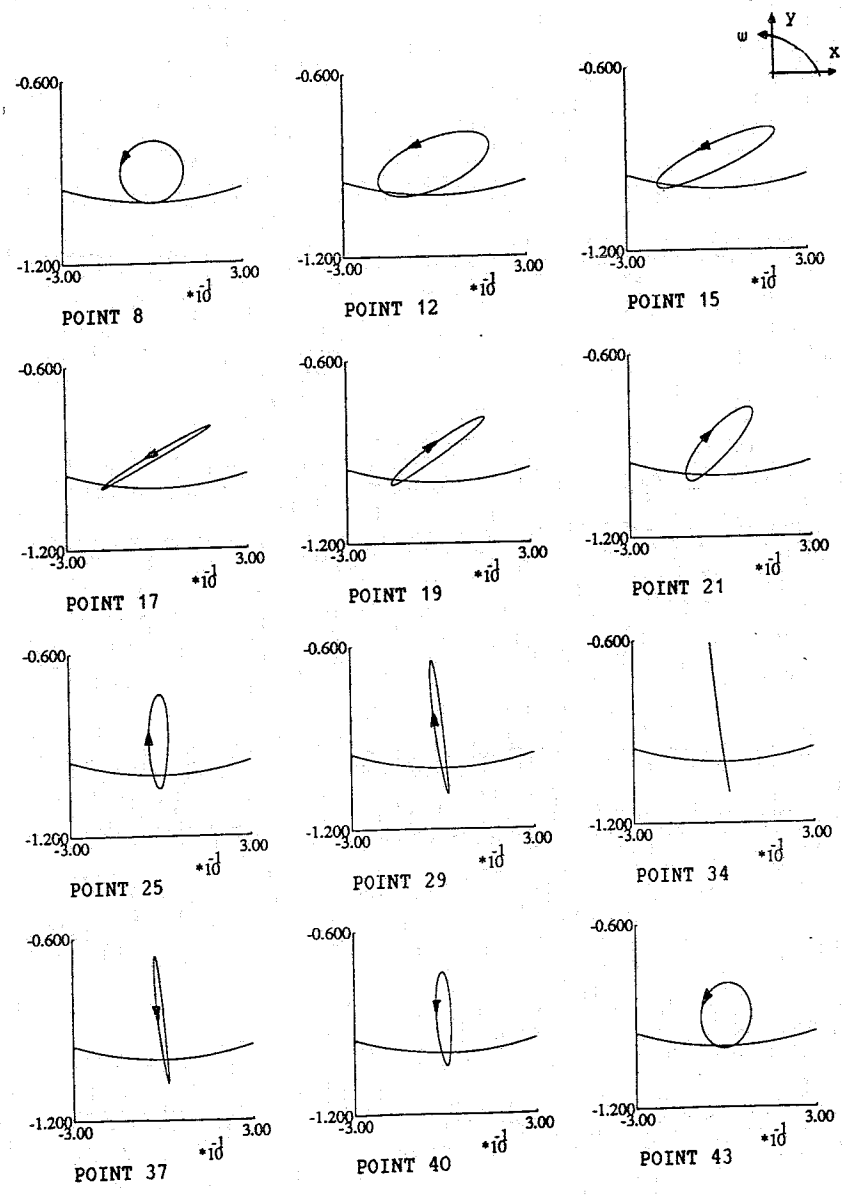


Fig 3 Motions described by the rotor centre $P_g$ in the x–y plane for the calculations given in Fig 2

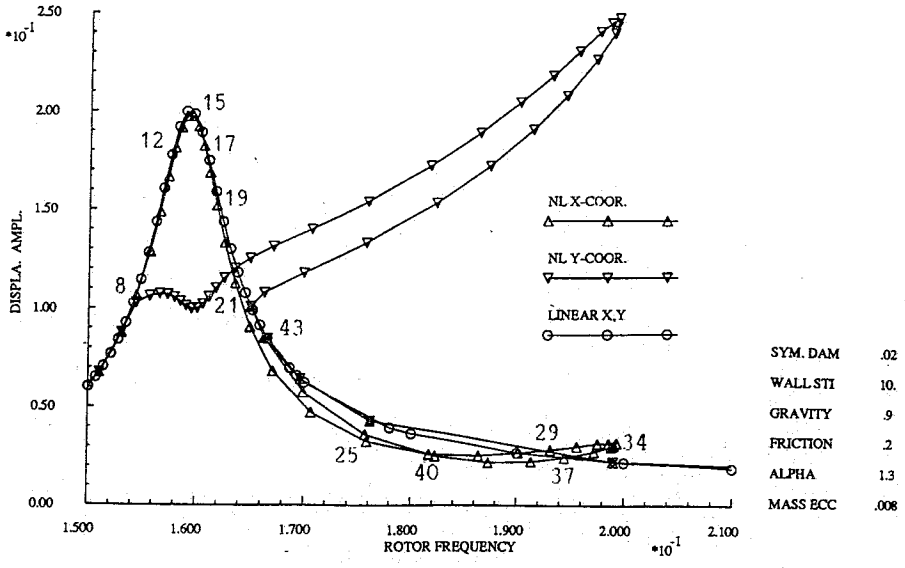


Fig 2 Amplitude of linear and non-linear orbits in the x and y directions

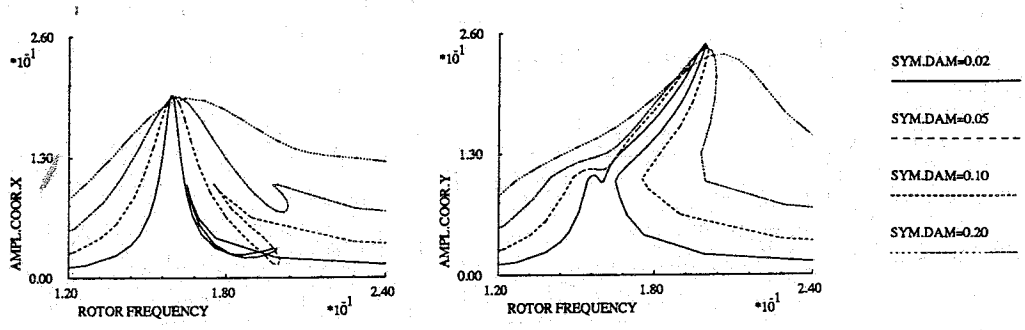


Fig 4 Influence of the damping $\varsigma$ on the amplitude of the coordinates in $\vec{e}_y$ directions for $F_r^* = 10$, $F_g^* = 0.9$, f = 0.2 and $\alpha = 1.3$

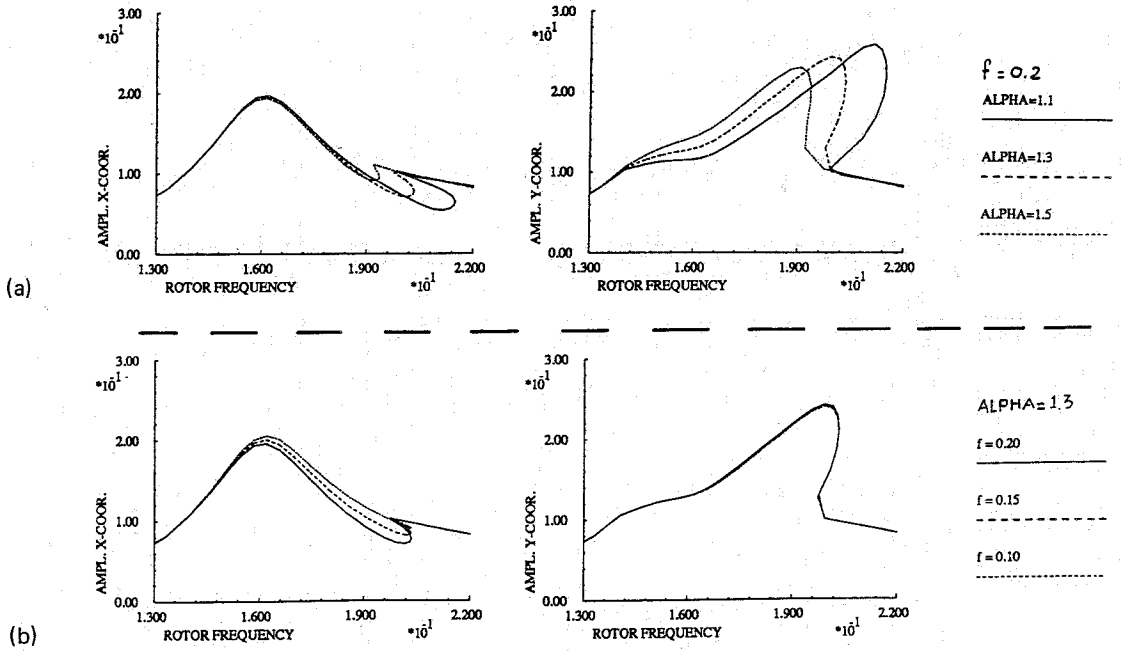


Fig 5 Influence of (a) $\alpha$ and (b) friction coefficient f on the amplitude of the coordinates in $\vec{e}_x$ and $\vec{e}_y$ directions for $\varsigma = 0.1$, $F_r^* = 1.0$, $F_g^* = 0.9$ and $\epsilon = 0.0398$